Elastic Membrane Heterogeneity of Living Cells Revealed by Stiff Nanoscale Membrane Domains

Charles Roduit,* F. Gisou van der Goot,† Paolo De Los Rios,‡ Alexandre Yersin,* Pascal Steiner,* Giovanni Dietler,§ Stefan Catsicas,* Frank Lafont,*¶ and Sandor Kasas§**

*Cellular Neurobiology Laboratory, Brain and Mind Institute, †Global Health Institute, ‡Institute of Theoretical Physics, and §Institute of Physics of Complex Matter, École Polytechnique Fédérale de Lausanne, Switzerland; ¶Biology Institute, Pasteur Institute, Lille, France; and **Département de Biologie Cellulaire et de Morphologie, Université de Lausanne, Switzerland

ABSTRACT Many approaches have been developed to characterize the heterogeneity of membranes in living cells. In this study, the elastic properties of specific membrane domains in living cells are characterized by atomic force microscopy. Our data reveal the existence of heterogeneous nanometric scale domains with specific biophysical properties. We focused on glycosylphosphatidylinositol (GPI)-anchored proteins, which play an important role in membrane trafficking and cell signaling under both physiological and pathological conditions and which are known to partition preferentially into cholesterol-rich microdomains. We demonstrate that these GPI-anchored proteins reside within domains that are stiffer than the surrounding membrane. In contrast, membrane domains containing the transferrin receptor, which does not associate with cholesterol-rich regions, manifest no such feature. The heightened stiffness of GPI domains is consistent with existing data relating to the specific condensation of lipids and the slow diffusion rates of lipids and proteins therein. Our quantitative data may forge the way to unveiling the links that exist between membrane stiffness, molecular diffusion, and signaling activation.

INTRODUCTION

The definition of heterogeneous plasma membrane compartments can influence our conception of many fundamental cell surface associated phenomena such as adhesion, the interaction of receptors with ligands, and susceptibility to infection. The property of the membrane adhesiveness is crucial for cell motility, cell-cell and cell-substratum contacts, the binding of ligands, and the invasion of pathogens. It depends on three parameters: the presence of lipids and proteins that interact with extracellular molecules, the subcortical cytoskeleton, and the intrinsic elastic properties of the plasma membrane. The first two parameters have been extensively studied using many biochemical and biophysical approaches. These approaches have been directed toward elucidating the diffusion kinetics of proteins and lipids within the bilayer and the impact of cytoskeletal dynamics thereupon (1). The third parameter can be analyzed with the highest resolution by atomic force microscopy (AFM) (2–4).

It has long been debated whether subcompartmentalization of the plasma membrane regulates the interaction of a cell with the extracellular environment (5,6). The fluid mosaic model proposed by Singer and Nicoloson in 1972 (7) has been revised to include membrane domains and cytoskeletal fences (1,8,9). The concept of membrane microdomains or lipid rafts was first proposed by Simons and Van Meer in 1988 (10). Within these cholesterol- and sphingolipid-enriched regions, specific proteins, such as glycosylphosphatidylinositol (GPI)-anchored ones and doubly acylated src-like kinases, are known to have high residency time (6,11). The proposed role of raft clustering in the triggering of signaling events (12) has shed new light on the dynamics of membrane-associated molecular assemblies. In the nervous system, these domains are believed to be of physiological importance in cell polarization and in the establishment and maintenance of neural network plasticity. Indeed, raft-associated signaling has been shown to be important for neuronal survival, for membrane polarity, and for neuritogenesis (13–16). For instance, during the establishment of neural networks, the interaction between the GPI domain, ephrin A, and Ephr mediated forward signaling and synapse formation (17). Rafts have also been implicated in several disorders of the nervous system, for instance in amyloidogenic processing of the Alzheimer β-amyloid precursor protein (18). The prion protein processes a GPI anchor, which is crucial for its trafficking and hence for its pathogenic conversion (19,20). Furthermore, several neurotoxins require raft-associated lipid species and/or proteins for their binding and entry (21). These include the botulinum (22), the cholera (23), and the tetanus toxins (24). Although protein-protein interactions occurring within these membrane domains have been shown to be crucial in establishing the immunological synapse (25), the mechanical properties of the rafts may regulate the partitioning dynamics of the proteins involved in signaling events.

GPI-anchored proteins represent a useful tool for studying cell surface domains. The surface distribution of GPI-anchored proteins, their diffusion rates, and their ability to associate with specific lipid domains have been studied in both biological and artificial membranes (1,26,27). Since their partitioning within rafts has been proposed to trigger activation cascades (12), these GPI-anchored proteins are

Submitted May 16, 2007, and accepted for publication October 1, 2007.

Frank Lafont and Sandor Kasas contributed equally to this work.

Address reprint requests to Sandor Kasas, E-mail: sandor.kasas@epfl.ch.

Editor: Peter Hinterdorfer.

0006-3495/08/02/1521/12 $2.00

doi: 10.1529/biophysj.107.112862

often used as a model to study signaling ''platforms'', namely, the stimulation-evoked clustering of signaling molecules (12). However, the mechanical properties of the membrane domain into which they are anchored are largely unknown. To establish whether a link exists between the functional role of GPI-anchored proteins and the molecular mechanism underlying signaling platform activation, it is necessary to better understand the biophysical properties of the so-called GPI domains. This information would also help us to characterize the dynamics of the cell surface receptor and of the ion channels mobilized during the establishment and maintenance of neuronal network.

AFM (28) permits an exploration of living material at high resolution. The instrument can image living cells (3,29,30) in a near physiological state and can measure their mechanical properties in the nanometer range (4,31–33). Using tips that have been functionalized with proteins, AFM can be applied to investigate protein-protein interaction forces (34–36). Recently this facility has been used to monitor the distribution of vitronectin receptor on living osteoblast membranes (37) and to map a virulence factor (heparin-binding hemagglutinin adhesin) on the surface of mycobacterium bacille Calmette-Guérin (38). The instrument has also been used to image the distribution of GPI domains in artificial membranes (for reviews, see Lagerholm et al. (2) and Henderson et al. (39)). Notwithstanding these advancements, quantitative data relating to the stiffness of cell membranes and especially to that of membrane microdomains are still lacking. We have recently demonstrated that AFM can also be used to selectively probe the mechanical properties of structures located at different depths in living cells (40). In this study, we describe an analytical method for estimating the relative membrane elasticity of living hippocampal neurones grown in primary cultures. We applied this method to analyze the relative plasma membrane elasticity of GPI domains in living hippocampal neurons.

MATERIALS AND METHODS

Cell culturing and drug treatment

Hippocampal neurones derived from rat embryos were prepared and cultured as previously described (41). The cells were plated in petri dishes at a numerical density of 2500/cm^2 and were maintained in K5 medium (128 mM NaCl, 5 mM KCl, 2.7 mM $CaCl_2$, 1 mM $MgCl_2$, 10 mM glucose, 20 mM HEPES (pH 7.4)) at ambient temperature. Each experiment was initiated 15 min after inserting the petri dish into the AFM. This delay was required for the thermal equilibration of the cantilever. When required, a 5 mM solution of MeCD in K5 was prepared and introduced into the incubation chamber using a homemade setup (42) to yield a final concentration of 2.5 mM. Cytochalasin B was likewise prepared in K5 to yield a final concentration of 5 μM.

Protein expression and tip coating

Proaerolysin and VSG117 were expressed and purified as previously described (43). Bovine serum albumin and wheat germ agglutinin (WGA) were purchased from Sigma (St. Louis, MO). The coating of mica plates and cantilevers was performed using an established protocol that preserved the functionality of the protein (36,44,45). The proteins were deposited at a concentration of 1 μg/ml. Aerolysin was used as a monomer.

AFM measurements and data processing

All experiments were performed at ambient temperature using a commercial stand-alone AFM (Bioscope, Veeco Instruments, Santa Barbara, CA), which was combined with an inverted optical microscope (Axiovert 200; Zeiss, Jena, Germany). We used a Veeco AFM cantilever with a nominal spring constant of 0.06 N/m and a nominal tip radius of curvature of 20 nm. The spring constant of the cantilever was determined using Veeco's calibration tools. The AFM was operated in the force-volume mode at a scanning frequency of 7 Hz. Using this operation mode, the tip periodically indents the sample during a scan. Hence, for each pixel that comprises an AFM image, the microscope sequentially records the deformation of the cantilever during a downward (extension) and an upward (retraction) movement of the tip. When the tip contacts the cell membrane, it deforms it by a 50-nm deflection of the cantilever. During the retraction part of the cycle, when the tip leaves the membrane, the maximal displacement was set at $\sim$1 μm above the cell. When such a cycle has been completed, the tip moves laterally to the next pixel to begin a new one. Owing to the considerable size of the data files (57 MB/files) generated by these measurements, the data were analyzed and statistically processed using our own software (developed under MATLAB 7.0; The MathWorks, Natick, MA) in conjunction with a GNU/Linux operating system. The software scanned each approach and retraction curve to compute Young's modulus. Binding-unbinding events on the retraction curve were detected according to their shape and size (Fig. 1 *B*) using a fuzzy logic algorithm (46). Young's modulus was computed using the Hertz model (47), which describes a sphere indenting a soft material (48). This model was applied to only a portion of the approach curve between the point of contact and the indentation to a depth of 50 nm. The point of contact between the AFM tip and the cell membrane was detected by the cantilever deflection according to the noise defined in the off contact part of the curve. In other words, we defined the contact as the spot on the force curve at which the vertical deflection of the cantilever overcomes the noise of the cantilever. For the *Er* calculation, adjacent pixels to the pixel in which a binding-unbinding event occurred were rejected when corresponding to substrate. Each experiment was performed at least five times. Statistical significances were evaluated using a two-tailed *t*-test.

RESULTS

Detection of GPI domains

For these experiments, fully mature (stage V) hippocampal neurones were used (49). The presence of GPI-anchored proteins within all neuronal compartments, viz., axons, soma, and dendrites, was established by fluorescence microscopy (see Supplementary Fig. S1). For the AFM analysis, we considered only neurites with a constant diameter of $\sim$1 μm (determined using an inverted optical microscope that was located beneath the AFM and using the AFM image (Bioscope I, Veeco)). The surfaces of the living cells were explored using the AFM in the force-volume imaging mode and in conjunction with tips coated with a GPI-anchor protein specific binding bacterial toxin aerolysin from *Aeromonas hydrophila* (Fig. 1 *A*). In this mode, the AFM successively records force-distance curves over the entire sample. When the aerolysin molecules interacted with proteins in the membrane, the cantilever was deflected during the retraction

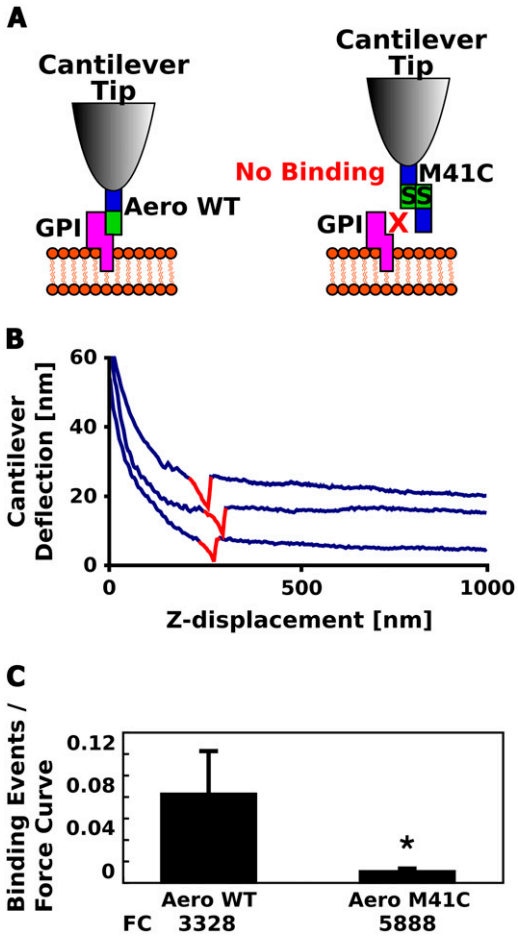

FIGURE 1 Binding specificity and distribution of binding events between aerolysin-functionalized tip and GPI domains. (*A*) Experimental setup describing the tip coated either with the aerolysin wild-type (Aero WT), which binds GPI domains on the cell membrane, or with the mutant M41C, which does not bind to GPI domains. (*B*) Force-distance curves examples. Force-distance curves recorded neurites with binding-unbinding events highlighted in red. (*C*) Number of binding-unbinding events/force curves with aerolysin (Aero WT)-coated tip and with the non-GPI domain binding mutant Aero M41C-coated tip tested on hippocampal neurones. The number of force curves (FC) analyzed is indicated. Data are mean ± SE; asterisk, $p < 0.03$, two-tailed *t*-test.

part of the force-distance curve. We refer to this slight, but characteristic movement of the cantilever as a binding-unbinding event. It indicates the presence of a ''GPI domain'' beneath the tip (Fig. 1 *B*).

Specific binding-unbinding events were common for tips functionalized with wild-type aerolysin but scarce for those coated with a binding-impaired mutant (M41C, Fig. 1 *C*), which forms disulphide-linked dimers (50). The latter finding also confirmed the absence of nonspecific binding associated with the coating procedure. As a further control, we determined whether the binding capacity of the aerolysin-coated tip was influenced during the course of neurite scanning (Supplementary Fig. S2).

Illustration of the methodology as applied to a single cell

Young's modulus was calculated by fitting the indentation curves obtained from the force-volume files to the Hertz model (see Materials and Methods). At zero force, topographic data (i.e., the three-dimensional image of the sample) were obtained by reading the piezzo z-position at the point of contact. Using our own software, the topographic data were combined with those pertaining to the absolute stiffness (see below) and to the position of the binding-unbinding events to yield images such as those depicted in Fig. 2 *A*. The membrane Young's modulii are shown in ''false'' colors, which are mapped on the cell surface topography in area units 2 μm × 2 μm with a resolution of 32 × 32 pixels. Pixels embracing a binding-unbinding event were considered ''GPI domains'' and are labeled with red arrows.

Fig. 2 *B* illustrates the pixels that were taken into consideration for the computation. Red stars indicate the regions in which binding-unbinding events occurred, which are referred to as GPI domains. Blue stars represent the surrounding region at distances of one, two, and three pixels from the GPI domain.

In Fig. 2, *C* and *D*, the mean stiffness values for the GPI domain (Fig. 2 *C*) and the three surrounding pixel regions are represented as a function of time. These data reveal no difference between the average stiffness of GPI domains (Fig. 2 *C*) and that of the surrounding membrane (Fig. 2 *D*). This finding reflects large-scale variations in cell stiffness, which result from local differences in topography (membranes appear stiffer near the periphery than close to the center of the cell) and organellar content and from the absence or presence of cytoskeletal filaments. To minimize these influences, we decided to consider only relative stiffness. This parameter was determined by dividing the absolute stiffness of each GPI domain (*red star*) by the stiffness of the surrounding membrane at distances of one, two, and three pixels (*blue stars*); i.e., for instance, at one pixel distance apart, the absolute stiffness of each GPI domain (*red star*) was divided by the mean of the absolute stiffness of the two pixels along the *x* axis immediately apposed (*blue stars*).

This type of measurement, therefore, only tells us to what extent a GPI domain is stiffer or softer than the membrane located around it. Considering the relative stiffness of the GPI domain instead of its absolute value has the advantage that there is no need to follow a specific domain from scan to scan. The physical properties are extracted from the statistical behavior of the whole GPI domains of the scan frame, and this ensemble can be used to determine the evolution of their properties as a function of time or as a function of chemicals, which could be added during the experiment. In addition, relative stiffness values can be directly compared and statistically processed independent of the location, the cell, and the moment when the measurement is accomplished.

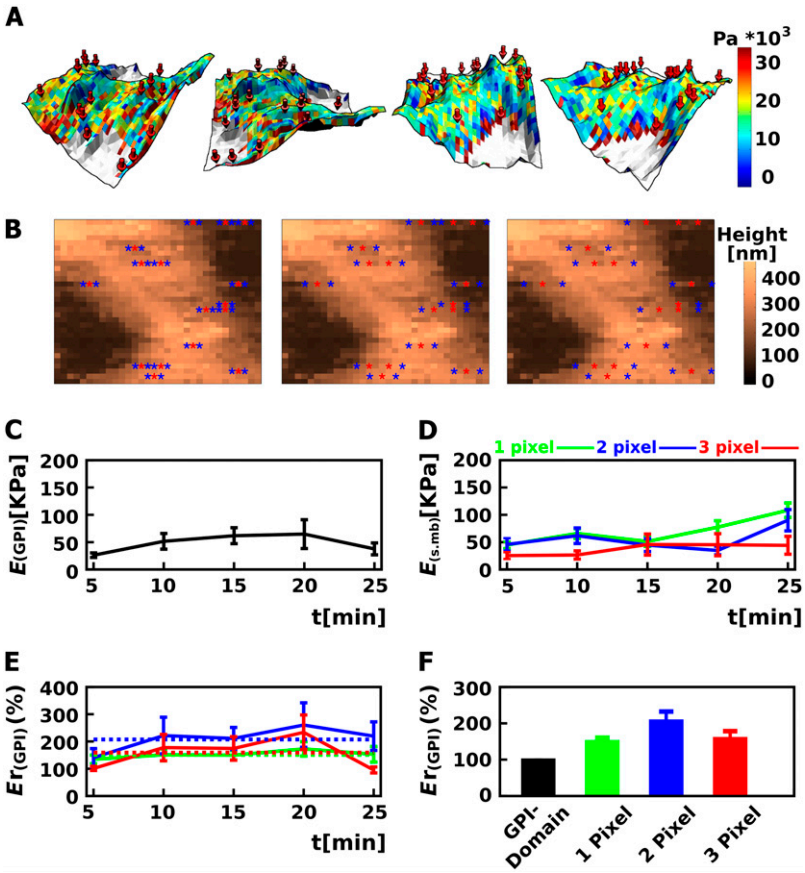

FIGURE 2 Young's modulus (E) measurements on a single neurite and determination of the relative Young's modulus (Er) of GPI domains. (*A*) Rotation series of three-dimensional reconstructed images showing the stiffness (expressed in Pascal (Pa) according to a false color scale) mapped on the topography. Red arrows indicate the location of GPI domains (specific events). (*B*) Topography (*A*, *top view*, *false colors*) with red stars indicating GPI domains and blue stars indicating the immediately surrounding membranes at one, two, and three pixel distances apart. (*C*) Absolute stiffness evolution of the GPI domains shown as a function of time ($E_{(GPI)}$). (*D*) Absolute stiffness values of the surrounding membrane ($E_{(s.mb)}$) at one, two, and three pixels (*green*, *blue*, and *red*, respectively). (*E*) Relative stiffness of GPI domains ($Er_{(GPI)}$) in percentage. For each binding-unbinding event, the $Er_{(GPI)}$ (*red star* in *B*) was calculated by dividing the $E_{(GPI)}$ by the mean of the $E_{(s.mb)}$ (*blue stars* in *B*) for the corresponding GPI domain at one, two, and three pixels apart (*green*, *blue*, and *red*, respectively). The mean of all the $Er_{(GPI)}$ was calculated and reported on the graph (12–30 values/time point). Data are mean ± SE. The means over the 25 min are indicated by dotted lines and reported on the histogram (*F*) together with the mean ± SE.

It is also well known that several cellular structures influence the mechanical properties of a cell (cytoskeleton, organelle, etc.). By indenting a cell with an AFM tip and by fitting the resulting indentation curve with the Hertz model, one integrates the mechanical contribution of the different structures present under the cell membrane. The resulting value therefore reflects the global mechanical contribution of all the actors and hides the particular role of the cell membrane, for example. To avoid interference with cellular structures located deep in the cell, we considered (i.e., we fitted with the Hertz model) only the first 50 nm of the indentation curve after the point of contact. This approach has recently been validated on the components of the cytoskeleton by Kasas and colleagues (40).

An additional difficulty with this type of measurement comes from the fact that membrane proteins and GPI domains move in the plane of the cell membrane and that, unfortunately, most of the currently available AFMs have a low scanning speed. We therefore compared only the stiffness of a GPI domain with the membrane located along the fast scan axis of the image (i.e., to the left and the right of the GPI domain in our images). This procedure reduces the number of reference measurements (pixels located around a GPI domain along the x axis but not the y axis) but increases the temporal resolution. With this compromise, the time required to measure GPI domain stiffness and its two surrounding reference points becomes reasonably short (420 ms at one pixel distance apart).

The measurement of the mechanical properties of the GPI domains is expressed on a relative stiffness scale: a value below 100 indicates that the pixel of interest is softer than the surrounding one; a value above 100 indicates that it is stiffer. In Fig. 2 *E*, the mean relative stiffness of all binding-unbinding events ($Er_{(GPI)}$) is depicted as a function of time. The green, blue, and red curves represent the stiffness of the GPI domains relative to that of the surrounding membrane at distances of one, two, and three pixels, respectively. This type of processing discloses only local changes in stiffness. The data reveal GPI domains to be stiffer than the surrounding membrane. The average relative stiffness values ($Er_{(GPI)}$) are depicted as a column in Fig. 2 *F* using the same color codes. In this single-cell experiment, the GPI domains were on average 40% stiffer than the surrounding membrane at a distance of one pixel (Fig. 2 *F*: *green bar*). This value reflects the statistical properties of the entire population of GPI domains within the analyzed scan frame; it does not correspond to the Er of a single GPI domain. Henceforth, all data are expressed as average values for several independent experiments (i.e., several independent cells).

The last step in the measurement of the mechanical properties of the GPI domains' stiffness consisted in the setup of different types of control experiments. The aim of these controls

was to verify that 1) the stiffness measurements were specific to the GPI domains, 2) the stiffness measurements were not influenced by the structures located underneath the membrane (cytoskeleton), 3) the presence of a protein attached to the tip that interacts with another protein located in the membrane does not influence the stiffness values obtained by our technique, 4) our measurements are also valid on a different cell line, and 5) the diffusion of the GPI domain proteins does not influence the measurements.

The fate of GPI domains after cholesterol extraction

GPI domains are known to be enriched in cholesterol, the extraction of which from the cell membrane induces their disruption. This event can be used to gauge the mechanical properties of the GPI domain in the AFM. We therefore applied the cholesterol-extracting drug, methyl-β-cyclodextrin (MeCD), to living neurones during time-lapse AFM measurements. MeCD has been used to study lipid rafts in living hippocampal neurones (14,51). Using this model, 40%–56% of the cholesterol was extracted using an MeCD concentration in the range 1–10 mM (23,52). In preliminary experiments, observation in the AFM revealed some shrinkage of neurites using an MeCD concentration of 5 mM. At 2.5 mM, no such effect was observed. Hence, we opted for the lower dose.

The $Er_{(GPI)}$ was monitored for 30 min after injecting medium alone (K5) and for 50 min after injecting MeCD into the cell chamber (Fig. 3 *A*, GPI domain). These graphs were obtained by averaging five experiments (i.e., five different cells). Intact GPI domains were stiffer than the surrounding

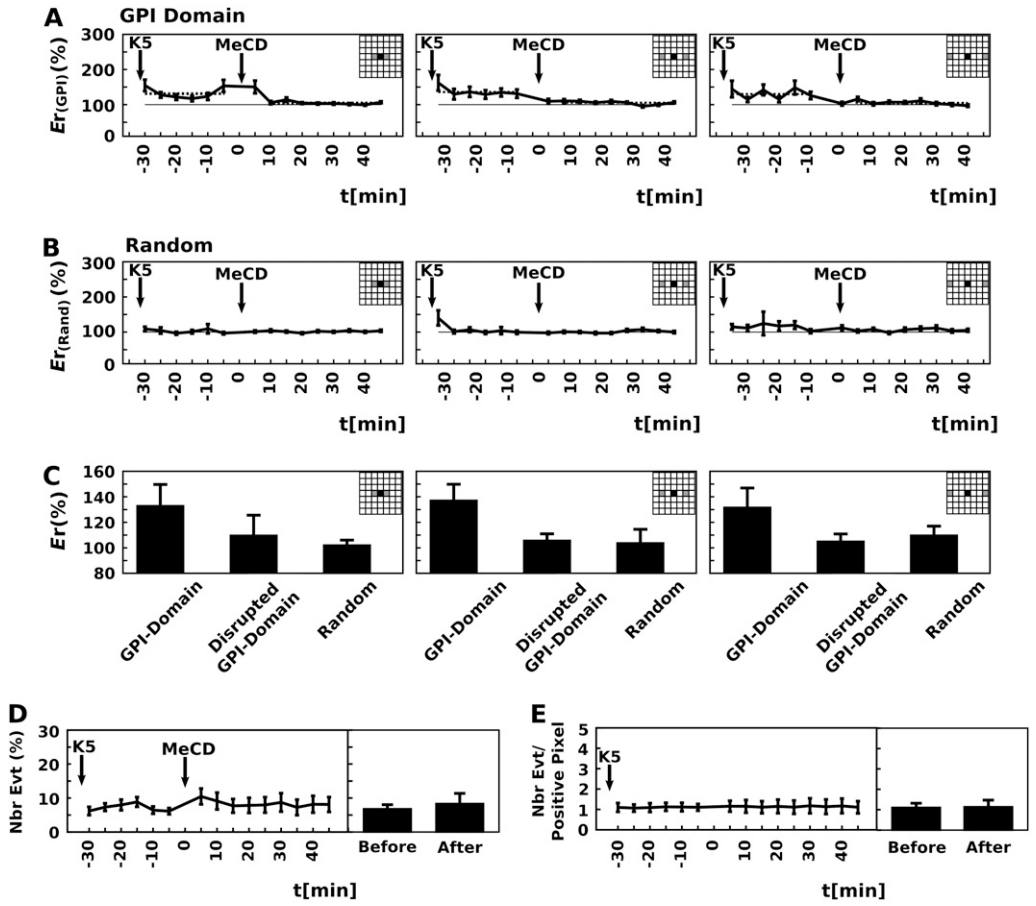

FIGURE 3 MeCD effect on the GPI domain relative stiffness. (*A*) $Er_{(GPI)}$ (GPI domain, *inset*: *black squares*) indicated in percentage and plotted as function of time before and after 2.5 mM MeCD injection. $Er_{(GPI)}$ are shown at one, two, and three pixels apart (*inset*: *gray squares*). The dotted line refers to the mean of $Er_{(GPI)}$ for the time periods (−30, −5) and (10–45) min. (*B*) $Er_{(Rand)}$ of randomly chosen pixels containing no detected GPI domains plotted as in *A*. (*C*) Histograms of the means of the $Er_{(GPI)}$ (GPI domain) and of the $Er_{(GPI)}$ after MeCD treatment (disrupted GPI domain) corresponding to the $Er_{(GPI)}$ over the (−30, −5) and (10–45) min periods shown in *A*, respectively, and of the $Er_{(Rand)}$ (random) shown in *B*. Five independent experiments were analyzed. Error bars indicate mean ± SE. (*D*) Mean of the total number of binding-unbinding events recorded with aerolysin-coated tips as a function of time. The means of the total number of binding events before and after MeCD injection are reported on the histogram. $p > 0.03$. (*E*) Mean of the number of binding events per positive pixel (i.e., in which binding-unbinding events occurred) as a function of time. The means of the number of binding-unbinding events per positive pixel before and after MeCD injection are reported on the histogram. Notice that for most pixels in which binding-unbinding events were detected only one specific event occurred. $p > 0.03$. Five independent experiments were analyzed. Error bars indicate mean ± SE.

membrane at a distance of one pixel ($p < 0.03$; $n = 5$). The injection of incubation medium (−30 min) had no influence on these relative stiffness values (no statistical difference was found when comparing $Er_{(GPI)}$ values before and after injecting the K5 medium over 30 min of recording ($N_{cells} = 5$, $p > 0.03$, *t*-test)). After treatment with MeCD, the stiffness of the GPI domains decreased to the same value recorded for the rest of the membrane (Fig. 2 *A*).

As an additional control, the GPI domains' relative stiffness, $Er_{(GPI)}$, was compared with the relative stiffness Er of randomly selected spots on the membrane ($Er_{(Rand)}$, Fig. 3 *B*, (random)). During analysis, GPI domains (i.e., spots with interactions) were excluded from the randomly selected data set. Compared with these randomly selected spots, GPI domains were found significantly stiffer at one pixel apart (~35% stiffer on average with $N_{cells} = 5$, $p < 0.03$, *t*-test) before MeCD treatment, (Fig. 3, *A* and *C*; Table 1). It should be noted that this value is consistent with the data shown in Fig. 2, which pertain to only a single cell. Importantly, treatment with MeCD elicited change neither in the total number of binding-unbinding events recorded (Fig. 3 *D*) nor in the number of events per positive force curve (Fig. 3 *E*).

Stiffness and size of the GPI domains

The size of raft domains is still debated (1,5,8,53). The data gleaned from our observations with the AFM revealed a significant change in Er between the GPI domains and the neighboring membrane at a distance of one pixel. Hence, the size of the GPI domain must be less than one pixel, i.e., ~70 nm in diameter; using a tip radius of 20 nm and a side angle of 35°, an indentation of 50 nm corresponds to a membranous domain ~70 nm in diameter. This value is in good agreement with the proposed sizes for GPI domains (see Discussion).

TABLE 1 Statistical analysis after drug treatment

	At 1 pixel	At 2 pixels	At 3 pixels
MeCD treatment (2.5 mM)			
Event K5 (−30 to −5) versus Event MeCD (10–45)	$p < 0.03$	$p < 0.03$	$p < 0.03$
Event K5 (−30 to −5) versus random	$p < 0.03$	$p < 0.03$	$p < 0.03$
Event MeCD (10–45) versus random	NS	NS	NS
Cytochalasin B treatment (5 μM)			
Event before versus after (30–90)	NS	NS	NS
Event after versus random (30–90)	$p < 0.03$	$p < 0.03$	$p < 0.03$

''Event K5'' corresponds to the injection of medium. Time intervals (in minutes) are indicated in parentheses. *p*-values were analyzed using the two-tailed *t*-test. NS, not significant.

Influence of the cytoskeleton on the stiffness of the GPI domains

The cellular membrane is underlain by a cortical network of actin, which is separated from the inner leaflet by a distance of a few nanometers (54). High-speed video microscopy has revealed lipids and proteins to diffuse within 100–200-nm diameter domains and to move from one domain to another. These domains were proposed to be delineated by an actin fence (1). The spatial and temporal resolution of our instrument did not permit us to confirm or refute this proposal. Nevertheless, we wished to assess the influence of the actin cytoskeleton on measurements of $Er_{(GPI)}$. To this end, we treated hippocampal neurones with cytochalasin B (5 μM), which depolymerizes the actin cytoskeleton. Treatment with cytochalasin B influenced neither the number of binding-unbinding events detected nor the number of events per positive curve ($p > 0.03$; $N_{cells} = 5$, data not presented). Remarkably, no difference in $Er_{(GPI)}$ was observed before and after actin depolymerization ($p > 0.03$ at a distance of one, two, and three pixels; $N_{cells} = 5$ (Fig. 4 *A*)). Even 30–90 min after treatment with cytochalasin B, the Er value was higher in GPI domains than in randomly selected control regions of the membrane ($p < 0.03$ at a distance of one, two, and three pixels; $N_{cells} = 5$; Fig. 4, *A* and *B*; Table 1). These data indicate not that the differences observed on GPI-anchored protein spots were exclusively the result of changes in the cytoskeleton but that our measurements also reflect the mechanical properties of the membrane itself. As can be seen in Fig. 4 *C*, after treatment with cytochalasin B, the difference between $Er_{(GPI)}$ and $Er_{(rand)}$ was less at a distance of one pixel than at two or three pixels (see Discussion).

To verify the effect of the cytochalasin on the absolute stiffness of the cell, Young's modulus of the cell compartment located within the scan frame was calculated. A statistically significant difference in this parameter was revealed with cytochalasin ($p < 0.03$; $N_{cells} = 5$), thereby demonstrating the actin cytoskeleton disrupting effect of the drug (Fig. 4 *D*).

This result shows that fitting only the very beginning of the indentation curve with the Hertz model is not enough to get rid of the actin cytoskeleton contribution. However, considering the relative stiffness instead of the absolute one permits us to detect differences in the membrane stiffness only.

Relative elasticity of the membrane near non-GPI-anchored proteins

It can be speculated that measurements of cell membrane stiffness are influenced by the interaction between proteins present on the tip and those located within the cell membrane. To refute the existence of this phenomenon, the tip was coated with an antibody against the transferrin receptor (TfR), which is documented to reside in non-GPI domains (6). These experiments revealed no differences between the Er values for TfR-containing domains and randomly selected

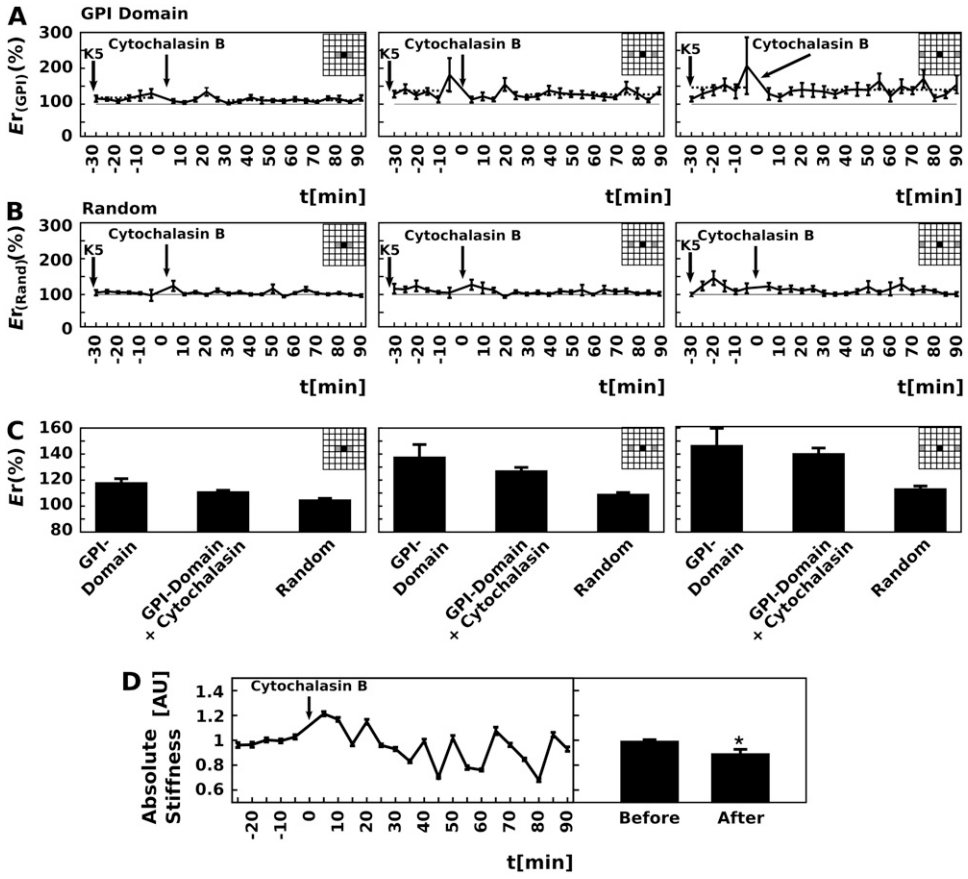

FIGURE 4 Actin depolymerization effects on the GPI domain relative stiffness and absolute membrane stiffness. (*A*) $Er_{(GPI)}$ (GPI domain, *inset*: *black squares*) indicated in percentage and plotted as a function of time before and after cytochalasin B treatment (5 μM). $Er_{(GPI)}$ are shown at one, two, and three pixels apart (*inset*: *gray squares*). The dotted line refers to the mean of $Er_{(GPI)}$ for the time period (−30, −5) and (30, 90) min. (*B*) $Er_{(RanI)}$ of randomly chosen pixels containing no detected GPI domains plotted as in *A*. (*C*) Histograms of the means of the $Er_{(GPI)}$ before (GPI domain) and after cytochalasin B treatment (GPI domain + cytochalasin) corresponding to the $Er_{(GPI)}$ over (−30, −5) and (30–90) min, respectively, shown in *A*, and of the $Er_{(Rand)}$ shown in *B* (random). (*D*) Absolute Young's modulus (absolute stiffness) of neurites treated with cytochalasin B. The average of Young's modulus for the pixels covering the entire neurite in the scan frame was calculated at each time point and then plotted as a function of time. Between 4,636 and 5,086 force curves were analyzed per time point with a total of 34,492 and 63,245 force curves analyzed for the time periods before and after cytochalasin B treatment, respectively. Time points for injection of K5 and MeCD are indicated by arrows on the plot. The means of the absolute stiffness (in arbitrary unit) before and after MeCD injection are reported on the histogram. Five independent experiments were analyzed. Error bars indicate mean ± SE.

control ones (Fig. 5). As a further control, we conducted measurements on neurones using tips functionalized with WGA. This protein binds sialic acid residues, which are homogeneously distributed on cell membranes. The *Er* values obtained for WGA-mediated binding-unbinding events were similar to those registered in randomly selected control regions at distances of one, two, and three pixels (Fig. 5). Hence, the greater stiffness of GPI domains compared to the surrounding regions of the membrane is apparently specific for this class of protein.

Cell line dependence

To exclude the peculiar behavior of hippocampal neurones, we repeated the same experiment with the 293T cell line derived from primary cultures of human embryonic kidney cells. Here again, we noticed that the GPI domains were stiffer and that a similar stiffness drop occurred after cholesterol extraction (Supplementary Fig. S3). The use of aerolysin offered the advantage of analyzing GPI-anchored proteins without discriminating any specific protein. However, to test whether similar results could indeed be obtained with a specific protein, we overexpressed a GPI-green fluorescent protein (GFP) construct in 293T cells and functionalized the tips with an anti-GFP antibody. In this case, the GPI-GFP domain had no significant difference in stiffness with the surrounding membrane at one pixel apart, which could be explained by the oligomerization of the construct. However, the GPI-GFP membrane domain appeared clearly stiffer than the surrounding membrane at two and three pixels apart (Supplementary Fig. S3).

Furthermore, after overexpression of the GPI-GFP construct by transient transfection in HeLa cells, we found again heightened values for theGPI domain versus the surrounding membrane when probing cells with aerolysin-functionalized tips (Supplementary Fig. S4).

After treatment with MeCD, the stiffness of the GPI domains decreased to the same value as that recorded for the rest of the membrane of neurones (Fig. 3 *A*) and of 293T and HeLa cells (Supplementary Figs. S3 and S4).

Influence of protein diffusion

It is very important to note that there are two timescales involved in the experiments. One is the time (5 min) required to take a full 2 × 2 micron size AFM image. The other

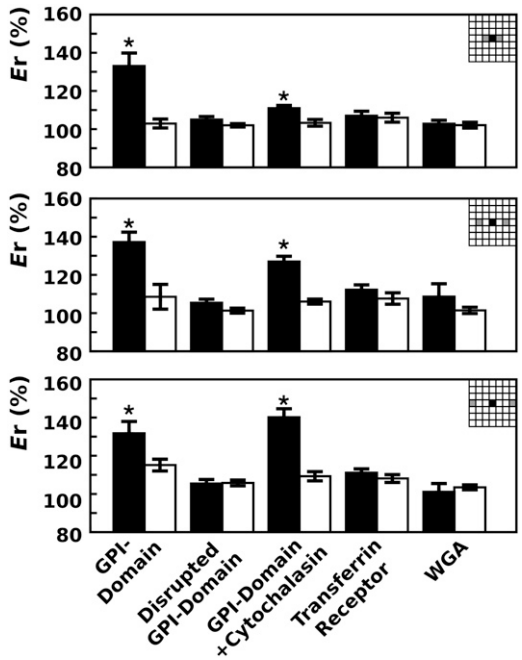

FIGURE 5 Comparison of the *Er* for GPI domains, transferrin-associated membrane, and WGA-associated membrane. Histograms indicate the mean of the *Er* calculated with aerolysin-coated tips for GPI domains, disrupted GPI domains (i.e., MeCD treated), and cytochalasin-treated GPI domains (data reported from Figs. 3 and 5). Means of the *Er* of the membrane recorded with anti-transferrin-coated tips and WGA-coated tips are also indicated. Means of the *Er* for the corresponding random controls are indicated in white filled boxes. The three histograms represent the results obtained when analyzing membranes located at one, two, and three pixels apart (see *insets*). Five independent experiments were analyzed. Error bars indicate mean ± SE.

timescale (140 ms), which is the most relevant in our experiment, relates to the time required to take one force curve on one pixel of the image. Previous studies have shown that clustered GPI-anchored proteins diffuse at 6×10^{-4} $\mu m^2/s$, whereas nonclustered GPI-anchored proteins diffuse more rapidly i.e., at 3.9 $\mu m^2/s$ (55). A relative stiffness measurement at one pixel distance requires 420 ms (700 ms at two and 980 ms at three pixels apart). During this time, clustered GPI-anchored proteins can diffuse over a surface of 2.52×10^{-4} μm^2. This surface corresponds to a circle with a 0.0179 μm diameter, whereas the AFM tip displacement is 0.1875 μm. The diffusion rate of the clustered GPI-anchored proteins is therefore one order of magnitude slower than the AFM tip to which the GPI-anchored proteins look as immobilized structures. To confirm this assumption, we repeated the experiments on HeLa cells that were fixed beforehand (paraformaldehyde (4%) treatment for 15 min at 4°C), which overexpressed GPI-GFP, and probed the cells with aerolysin-coated tips. We obtained similar results as for the overexpressed 293T cells. GPI domains appeared stiffer than the surrounding membrane, whereas treatments with MeCD before cell fixation decreased the relative stiffness to the same value as the surrounding membrane (Supplementary Fig. S4).

DISCUSSION

In this work, we present a methodology we developed to assess cell membrane local mechanical properties. The method was successfully applied to living neurons and permitted us to estimate the average GPI domain size as well as their average mechanical properties.

GPI-anchored proteins are known to interact with aerolysin, which we used to coat the AFM tip. The specificity of this interaction has been assessed by the use of a binding-impaired mutant, which does not bind to the proteins of the GPI domains. The experiments in which this mutant was attached to the AFM tip gave a dramatically reduced number of interactions as compared to those in which the wild-type of aerolysin was used. As a second control, we also used antibodies directed against a single protein, the GPI-GFP chimera. The interaction's specificity was similar to the one obtained with the aerolysin. Using fluorescence resonance energy transfer, Mayor et al. have shown that 20%–40% of GPI-anchored proteins form cholesterol-dependent clusters 4–5 nm in size with at most four molecules per cluster at resting state (53). Our detection method did not allow us to discriminate among monomers, dimers, and clusters; this discrimination remains extremely challenging with AFM on living cells and will be addressed specifically in a future work.

The measurement of the mechanical properties of the GPI domains was the major challenge of this project. The two major difficulties we faced were the specific measurement of the cell membrane and the large stiffness variations occurring over the surface of living cells. The first issue was addressed by considering only the first 50 nm of the indentation curve. This permitted us to restrict the measurement depth to the surface of the cell. Concerning the second issue, it is well known that the cell stiffness changes dramatically all over the cellular surface and that thermal drift of the instrument, creep, or motions of the cell dramatically compromise any attempt to measure subtle stiffness variations. We therefore did not measure the absolute stiffness of a single GPI domain; rather we compared its stiffness with the stiffness of the spots located in its immediate vicinity that were not identified as GPI domains (i.e., with no interactions). The use of relative stiffness thus allowed us to eliminate several problems, including those previously mentioned and others, such as the topology of the cell, the height of the cytoplasm above the substrate, the large-scale local stiffness variations, and the requirement to follow the same domain after successive scans. By considering the relative stiffness, it became possible to compare and to average the different values; the data we present here, therefore, reflect the statistical behavior of thousands of GPI domains. For these measurements, we made the assumption that there was no correlation between adjacent pixels. This is based on the notion that the smallness of the tip

(nominal tip radius of curvature = 20 nm) should not introduce pixel correlation beyond one pixel distance (62.5 nm). Pixel correlation should have led to reproducible results independent of the treatment and the tip coating.

Another important issue is the time resolution of the method, whose influence has been minimized by considering only the neighboring pixels located along the microscope's fast scanning axis. Thus a measurement at one pixel distance required only 420 ms per binding-unbinding event, as GPI-anchored proteins were documented to move much slower.

To exclude the possibility that the stiffness of the GPI domains we measured is induced by the specific interaction between the proteins coated onto tips and those inserted into the membrane (i.e., aerolysin and the GPI domain proteins), we disrupted the GPI domains by using MeCD, a chemical compound that is known to extract the cholesterol from the membrane while leaving the GPI proteins unaffected. The experimental results clearly show that without cholesterol, GPI domains recover the same stiffness as the rest of the membrane, whereas the number of interactions remained unchanged, increasing the plausibility of our method. Our results are also in agreement with earlier studies on the role of cholesterol on artificial membranes' stiffness (56).

As a further control we coated the AFM tip with antibodies directed against a specific protein (GPI-GFP) of the GPI domain (at variance with aerolysin, which interacts with several of them) and obtained similar results. Moreover, the experiments were repeated with AFM tips coated with anti-TfR antibodies. TfR was chosen because it is known to be excluded from the GPI domains. The relative stiffness of the TfR-anti-TfR antibody interaction spots was the same as that obtained on the randomly selected spots. This experiment therefore demonstrated again that the stiffness increase we previously measured on GPI domains is specific to the domains and does not reflect any putative increase in the stiffness, which would be induced by the creation of a link between the tip and the cell membrane.

The last point that remained to be elucidated was whether the GPI domains' stiffness that we measured was a consequence of the actin cytoskeleton filaments that are present underneath the membrane. We therefore exposed the cells to cytochalasin (or latrunculin, data not shown), a chemical known to affect actin filaments. Here again, the GPI domains' relative stiffness was higher than the rest of the membrane whether the actin cytoskeleton was disrupted or not. The cytochalasin action was confirmed by the fact that the absolute stiffness of the all scan frame dropped significantly after injection, in agreement with Rotsch and Radmacher (57). This last point demonstrates that considering the first 50 nm of the indentation curve permits us not only to measure the stiffness of the cell membrane (by relative measurements) but also to apprehend the actin cytoskeleton (by absolute measurements). It should be noted that the absolute stiffness of the overall scanned area did not significantly vary after cyclodextrin injection, the treatment that extracts cholesterol but has no action on the actin filaments.

To verify the contribution of protein diffusion to our results, we repeated the experiments on fixed HeLa cells where all protein diffusion is definitely absent. Results were very similar to those in the living cells. The stiffness differences were, however, less important than those on living HeLa cells, probably due to the fixation procedure where all proteins are cross-linked.

In a final control we repeated our experiments on a second different cell line (293T cells) and obtained similar results to those of the presented experiments on neurones.

The relative stiffness measurements thus revealed that that GPI domains are 30% stiffer than the rest of the membrane. It should be pointed out that the method used here does not exclude the possibility that the GPI domains are even stiffer than the value we actually measured. This is due to a phenomenon that can be illustrated by a coin glued to the surface of an inflated balloon. The balloon stiffness one measures by pushing on the coin appears to be greater than the stiffness of the rest of the balloon, but this apparent stiffness is far lower than that of the coin itself.

The measurements also permitted us to estimate the size of the GPI domains according to their stiffness difference with the surrounding membrane. The domains were found to be $<$70 nm, in agreement with the reported size for these domains using other approaches (1,6,8,53) and AFM on artificial membranes (58).

Our study validates AFM to investigate GPI domains and membrane subdomains in living cells, in addition to the various biochemical techniques that have been used previously (e.g., (59,60)). These techniques strongly depend on the detergent used to isolate membrane subdomains (61) and therefore require complementary approaches (62,63) such as AFM.

These observations not only provided mechanical information on different membrane regions, but they also confirmed the existence of submicron domains in the plasma membrane of living cells, an issue that has recently been heavily debated (5).

Several lines of evidence argue that the dynamics of rafts likely depends on the actin cytoskeleton (64,65), an issue that we did not address here. Kusumi et al. have proposed a model, called the actin fence and picket model, based on actin subcompartmentalization of the cell membrane (30–300 nm depending on the cell type (for a review see Kusumi et al. (1)). The membrane compartmentalization by actin cytoskeleton is comparable to the diffusion confinement of phospholipids (54). It has been proposed that lipid rafts may define confinement zones within these compartments. We noticed that the $Er_{(GPI)}$ after cytochalasin B treatment became lower at one pixel than at two and three pixels apart. This would imply that the size of the GPI domains had increased without a change in stiffness. This remains an open issue at this stage and requires further analysis.

One main goal of this study was to determine whether AFM could detect a difference in the stiffness of membrane domains in living cells. This is an important point in the context of the debated issue of the behavior of proteins and lipids in raft microdomains. This approach allows us to address the issue of the relationships between membrane mechanical properties as stiffness, membrane structure, and protein and lipid diffusion. It is clear that raft-associated protein-protein interaction may participate in driving molecular assemblies, as suggested by the work of Douglass and Vale (25), though participation of the lipid environment is not excluded. Here, we focused on GPI-anchored proteins; oligomerization of GPI-anchored protein is also under discussion (53,66).

Whether oligomerization of GPI-anchored proteins affects the lateral diffusion and the stiffness of the membrane into which they distribute is beyond the scope of this study but is certainly a next step to investigate. We demonstrated that the GPI domains are stiffer than the surrounding membrane, and many reports have documented that the diffusion of lipids and proteins are slower in so-called raft microdomains on living cells (1,26) and artificial membranes (27). Using the probe Laurdan, Gauss et al. have demonstrated that rafts can form condensed domains on living cells (67). It is thus attractive to propose that the stiff areas we observed correspond to specific platforms into which the diffusion of these lipids and proteins is modified, allowing the formation of signaling complexes involved in a variety of raft-dependent physiological events and infectious diseases (21,27). A prediction of this hypothesis is that lowering changes in stiffness between domains should impair signaling. Indeed, several reports have shown that upon MeCD activation of signaling, cascades are inhibited (12). Interestingly, ganglioside overexpression has been documented to decrease membrane fluidity and to suppress the neurotrophic tyrosine kinase receptor type 1-dependent signaling activation upon nerve growth factor (NGF) treatment (68). More studies are obviously needed to understand the physics of the relationship between diffusion and stiffness. However, our data strongly suggest that differences in stiffness clearly occur in biological membranes and that one class of proteins often considered raft-associated, i.e., GPI-anchored proteins, partitions into stiff domains.

Altogether these results demonstrate that it is possible to measure the relative stiffness of plasma membrane domains in living cells. The method described here thus provides perspectives for investigating biophysical properties of the cell plasma membrane with a broad spectrum of applications. It permits us to study, at the nanometrical level, the role of adhesion mechanisms on the membranes of living cells. Further applications could include the study of mechanical properties of receptors before and after stimulation with physiological ligands or pharmaceutical compounds. Hence, a link can be established between the mechanical properties of the lipid bilayer and the fate of surface proteins, leading to signaling activation and shedding new light on the study of membrane-coupled signal transduction.

SUPPLEMENTARY MATERIAL

To view all of the supplemental files associated with this article, visit www.biophysj.org.

We thank L. Glauser for her assistance with cell culturing, J.-P. Aimé, H. Markram, and D. J. Müller for their constructive suggestions, and L. Forrò, J. Gruenberg, and K. Simons for their critical reading of early versions of the manuscript. F.L. thanks D. Trono for his encouragement and support.

This work was supported by grants from the Swiss National Science Foundation (to G.v.d.G. and S.C.), the European Molecular Biology Organization Young Investigator Program, and the National Institutes of Health (to G.v.d.G.). F.L. is the recipient of grants from the French Minister of Research and new Technologies (MENRT) and the Fondation pour la Recherche Médicale (FRM).

REFERENCES

1. Kusumi, A., I. Koyama-Honda, and K. Suzuki. 2004. Molecular dynamics and interactions for creation of stimulation-induced stabilized rafts from small unstable steady-state rafts. *Traffic*. 5:213–230.
2. Lagerholm, B. C., G. E. Weinreb, K. Jacobson, and N. L. Thompson. 2005. Detecting microdomains in intact cell membranes. *Annu. Rev. Phys. Chem.* 56:309–336.
3. Milhiet, P., M. Giocondi, and G. C. Le. 2003. AFM imaging of lipid domains in model membranes. *ScientificWorldJournal*. 3:59–74.
4. Weisenhorn, A. L., M. Khorsandi, S. Kasas, V. Gotzos, and H.-J. Butt. 1993. Deformation and height anomaly of soft surfaces studied with an AFM. *Nanotechnology*. 4:106–113.
5. Munro, S. 2003. Lipid rafts: elusive or illusive? *Cell*. 115:377–388.
6. Simons, K., and E. Ikonen. 1997. Functional rafts in cell membranes. *Nature*. 387:569–572.
7. Singer, S. J., and G. L. Nicolson. 1972. The fluid mosaic model of the structure of cell membranes. *Science*. 175:720–731.
8. Anderson, R. G., and K. Jacobson. 2002. A role for lipid shells in targeting proteins to caveolae, rafts, and other lipid domains. *Science*. 296:1821–1825.
9. Edidin, M. 2003. The state of lipid rafts: from model membranes to cells. *Annu. Rev. Biophys. Biomol. Struct.* 32:257–283.
10. Simons, K., and G. van Meer. 1988. Lipid sorting in epithelial cells. *Biochemistry*. 27:6197–6202.
11. Brown, D., and E. London. 1998. Functions of lipid rafts in biological membranes. *Annu. Rev. Cell Dev. Biol.* 14:111–136.
12. Simons, K., and D. Toomre. 2000. Lipid rafts and signal transduction. *Nat. Rev. Mol. Cell Biol.* 1:31–39.
13. Guirland, C., S. Suzuki, M. Kojima, B. Lu, and J. Q. Zheng. 2004. Lipid rafts mediate chemotropic guidance of nerve growth cones. *Neuron*. 42:51–62.
14. Ledesma, M. D., B. Brugger, C. Bunning, F. T. Wieland, and C. G. Dotti. 1999. Maturation of the axonal plasma membrane requires upregulation of sphingomyelin synthesis and formation of protein-lipid complexes. *EMBO J*. 18:1761–1771.
15. Niethammer, P., M. Delling, V. Sytnyk, A. Dityatev, K. Fukami, and M. Schachner. 2002. Cosignaling of NCAM via lipid rafts and the FGF receptor is required for neuritogenesis. *J. Cell Biol.* 157: 521–532.
16. Tansey, M. G., R. H. Baloh, J. Milbrandt, and E. M. J. Johnson. 2000. GFRalpha-mediated localization of RET to lipid rafts is required for effective downstream signaling, differentiation, and neuronal survival. *Neuron*. 25:611–623.
17. Scheiffele, P. 2003. Cell-cell signaling during synapse formation in the CNS. *Annu. Rev. Neurosci.* 26:485–508.

18. Ehehalt, R., P. Keller, C. Haass, C. Thiele, and K. Simons. 2003. Amyloidogenic processing of the Alzheimer beta-amyloid precursor protein depends on lipid rafts. *J. Cell Biol.* 160:113–123.

19. Brugger, B., C. Graham, I. Leibrecht, E. Mombelli, A. Jen, F. Wieland, and R. Morris. 2004. The membrane domains occupied by glycosylphosphatidylinositol-anchored prion protein and Thy-1 differ in lipid composition. *J. Biol. Chem.* 279:7530–7536.

20. Taraboulos, A., M. Scott, A. Semenov, D. Avrahami, L. Laszlo, and S. B. Prusiner. 1995. Cholesterol depletion and modification of COOH-terminal targeting sequence of the prion protein inhibit formation of the scrapie isoform. *J. Cell Biol.* 129:121–132.

21. Lafont, F., L. Abrami, and F. G. van der Goot. 2004. Bacterial subversion of lipid rafts. *Curr. Opin. Microbiol.* 7:4–10.

22. Lalli, G., S. Bohnert, K. Deinhardt, C. Verastegui, and G. Schiavo. 2003. The journey of tetanus and botulinum neurotoxins in neurons. *Trends Microbiol.* 11:431–437.

23. Shogomori, H., and A. H. Futerman. 2001. Cholesterol depletion by methyl-beta-cyclodextrin blocks cholera toxin transport from endosomes to the Golgi apparatus in hippocampal neurons. *J. Neurochem.* 78:991–999.

24. Herreros, J., T. Ng, and G. Schiavo. 2001. Lipid rafts act as specialized domains for tetanus toxin binding and internalization into neurons. *Mol. Biol. Cell.* 12:2947–2960.

25. Douglass, A. D., and R. D. Vale. 2005. Single-molecule microscopy reveals plasma membrane microdomains created by protein-protein networks that exclude or trap signaling molecules in T cells. *Cell.* 121: 937–950.

26. Mayor, S., and M. Rao. 2004. Rafts: scale-dependent, active lipid organization at the cell surface. *Traffic.* 5:231–240.

27. Simons, K., and W. L. C. Vaz. 2004. Model systems, lipid rafts, and cell membranes. *Annu. Rev. Biophys. Biomol. Struct.* 33:269–295.

28. Binnig, G., H. Rohrer, C. Gerber, and E. Weibel. 1982. Tunneling through a controllable vacuum gap. *Appl. Phys. Lett.* 40:178–180.

29. Kasas, S., V. Gotzos, and M. R. Celio. 1993. Observation of living cells using the atomic force microscope. *Biophys. J.* 64:539–544.

30. Radmacher, M., R. W. Tillamnn, M. Fritz, and H. E. Gaub. 1992. From molecules to cells: imaging soft samples with the atomic force microscope. *Science.* 257:1900–1905.

31. Radmacher, M., M. Fritz, C. M. Kacher, J. P. Cleveland, and P. K. Hansma. 1996. Measuring the viscoelastic properties of human platelets with the atomic force microscope. *Biophys. J.* 70:556–567.

32. Tao, N. J., S. M. Lindsay, and S. Lees. 1992. Measuring the microelastic properties of biological material. *Biophys. J.* 63:1165–1169.

33. Weisenhorn, A., P. Maivald, H. Butt, and P. Hansma. 1992. Measuring adhesion, attraction, and repulsion between surfaces in liquids with an atomic-force microscope. *Phys. Rev. B Condens. Matter.* 45:11226–11232.

34. Florin, E. L., V. T. Moy, and H. E. Gaub. 1994. Adhesion forces between individual ligand-receptor pairs. *Science.* 264:415–417.

35. Hinterdorfer, P., W. Baumgartner, H. Gruber, K. Schilcher, and H. Schindler. 1996. Detection and localization of individual antibody-antigen recognition events by atomic force microscopy. *Proc. Natl. Acad. Sci. USA.* 93:3477–3481.

36. Yersin, A., H. Hirling, P. Steiner, S. Magnin, R. Regazzi, B. Huni, P. Huguenot, P. De los Rios, G. Dietler, S. Catsicas, and S. Kasas. 2003. Interactions between synaptic vesicle fusion proteins explored by atomic force microscopy. *Proc. Natl. Acad. Sci. USA.* 100:8736–8741.

37. Kim, H., H. Arakawa, T. Osada, and A. Ikai. 2003. Quantification of cell adhesion force with AFM: distribution of vitronectin receptors on a living MC3T3-E1 cell. *Ultramicroscopy.* 97:359–363.

38. Dupres, V., F. D. Menozzi, C. Locht, B. H. Clare, N. L. Abbott, S. Cuenot, C. Bompard, D. Raze, and Y. F. Dufrene. 2005. Nanoscale mapping and functional analysis of individual adhesins on living bacteria. *Nat. Methods.* 2:515–520.

39. Henderson, R. M., J. M. Edwardson, N. A. Geisse, and D. E. Saslowsky. 2004. Lipid rafts: feeling is believing. *News Physiol. Sci.* 19:39–43.

40. Kasas, S., X. Wang, H. Hirling, R. Marsault, B. Huni, A. Yersin, R. Regazzi, G. Grenningloh, B. Riederer, L. Forro, G. Dietler, and S. Catsicas. 2005. Superficial and deep changes of cellular mechanical properties following cytoskeleton disassembly. *Cell Motil. Cytoskeleton.* 62:124–132.

41. Morgenthaler, F. D., G. W. Knott, J. Floyd Sarria, X. Wang, J. K. Staple, S. Catsicas, and H. Hirling. 2003. Morphological and molecular heterogeneity in release sites of single neurons. *Eur. J. Neurosci.* 17:1365–1374.

42. Kasas, S., X. Wang, H. Hirling, S. Catsicas, C. Haeberli, G. Dietler, and N. Thomson. 2000. Setup for observing living cells using a commercial atomic force microscope. *Rev. Sci. Instrum.* 71:4338–4340.

43 Abrami, L., M. C. Velluz, Y. Hong, K. Ohishi, A. Mehlert, M. Ferguson, T. Kinoshita and F. Gisou van der Goot. 2002. The glycan core of GPI-anchored proteins modulates aerolysin binding but is not sufficient: the polypeptide moiety is required for the toxin-receptor interaction. *FEBS Lett.* 512:249–254.

44. Allen, S., X. Chen, J. Davies, M. C. Davies, A. C. Dawkes, J. C. Edwards, C. J. Roberts, J. Sefton, S. J. Tendler, and P. M. Williams. 1997. Detection of antigen-antibody binding events with the atomic force microscope. *Biochemistry.* 36:7457–7463.

45. Allen, S., J. Davies, M. C. Davies, A. C. Dawkes, C. J. Roberts, S. J. Tendler, and P. M. Williams. 1999. The influence of epitope availability on atomic-force microscope studies of antigen-antibody interactions. *Biochem. J.* 341:173–178.

46. Kasas, S., B. M. Riederer, S. Catsicas, B. Cappella, and G. Dietler. 2000. Fuzzy logic algorithm to extract specific interaction forces from atomic force microscopy data. *Rev. Sci. Instrum.* 71:2082–2086.

47. Hertz, H. 1882. Über die Berührung fester elastischer Körper. *Journal für die reine und angewandte Mathematik.* 92:156–171.

48. Radmacher, M. 1997. Measuring the elastic properties of biological samples with the AFM. *IEEE Eng. Med. Biol. Mag.* 16:47–57.

49. Dotti, C. G., C. A. Sullivan, and G. A. Banker. 1988. The establishment of polarity by hippocampal neurons in culture. *J. Neurosci.* 8:1454–1468.

50. Hardie, K. R., A. Schulze, M. W. Parker, and J. T. Buckley. 1995. Vibrio spp. secrete proaerolysin as a folded dimer without the need for disulphide bond formation. *Mol. Microbiol.* 17:1035–1044.

51. Ledesma, M. D., K. Simons, and C. G. Dotti. 1998. Neuronal polarity: essential role of protein-lipid complexes in axonal sorting. *Proc. Natl. Acad. Sci. USA.* 95:3966–3971.

52. Sooksawate, T., and M. A. Simmonds. 2001. Effects of membrane cholesterol on the sensitivity of the GABA(A) receptor to GABA in acutely dissociated rat hippocampal neurones. *Neuropharmacology.* 40:178–184.

53 Sharma, P., R. Varma, R. C. Sarasij, Ira, K. Gousset, G. Krishnamoorthy, M. Rao, and S. Mayor. 2004. Nanoscale organization of multiple GPI-anchored proteins in living cell membranes. *Cell.* 116:577–589.

54. Morone, N., T. Fujiwara, K. Murase, R. S. Kasai, H. Ike, S. Yuasa, J. Usukura, and A. Kusumi. 2006. Three-dimensional reconstruction of the membrane skeleton at the plasma membrane interface by electron tomography. *J. Cell Biol.* 174:851–862.

55. Nohe, A., E. Keating, M. Fivaz, F. G. van der Goot, and N. O. Petersen. 2006. Dynamics of GPI-anchored proteins on the surface of living cells. *Nanomedicine.* 2:1–7.

56. Needham, D., and R. S. Nunn. 1990. Elastic deformation and failure of lipid bilayer membranes containing cholesterol. *Biophys. J.* 58:997–1009.

57. Rotsch, C., and M. Radmacher. 2000. Drug-induced changes of cytoskeletal structure and mechanics in fibroblasts: an atomic force microscopy study. *Biophys. J.* 78:520–535.

58. Tokumasu, F., A. J. Jin, G. W. Feigenson, and J. A. Dvorak. 2003. Nanoscopic lipid domain dynamics revealed by atomic force microscopy. *Biophys. J.* 84:2609–2618.

59. Brown, D. A., and J. K. Rose. 1992. Sorting of GPI-anchored proteins to glycolipid-enriched membrane subdomains during transport to the apical cell surface. *Cell.* 68:533–544.

60. Lafont, F., and K. Simons. 2001. Raft-partitioning of the ubiquitin ligases Cbl and Nedd4 upon IgE-triggered cell signaling. *Proc. Natl. Acad. Sci. USA*. 98:3180–3184.

61. Schuck, S., M. Honsho, K. Ekroos, A. Shevchenko, and K. Simons. 2003. Resistance of cell membranes to different detergents. *Proc. Natl. Acad. Sci. USA*. 100:5795–5800.

62. Harder, T., and K. Simons. 1997. Caveolae, DIGs, and the dynamics of sphingolipid-cholesterol microdomains. *Curr. Opin. Cell Biol.* 9:534–542.

63. Schutz, G. J., G. Kada, V. P. Pastushenko, and H. Schindler. 2000. Properties of lipid microdomains in a muscle cell membrane visualized by single molecule microscopy. *EMBO J.* 19:892–901.

64. Golub, T., and C. Pico. 2005. Spatial control of actin-based motility through plasmalemmal PtdIns(4,5)P_2-rich raft assemblies. *Biochem. Soc. Symp.* 72:119–127.

65. Harder, T., and K. Simons. 1999. Clusters of glycolipid and glycosylphosphatidylinositol-anchored proteins in lymphoid cells: accumulation of actin regulated by local tyrosine phosphorylation. *Eur. J. Immunol.* 29:556–562.

66. Glebov, O. O., and B. J. Nichols. 2004. Lipid raft proteins have a random distribution during localized activation of the T-cell receptor. *Nat. Cell Biol.* 6:238–243.

67. Gaus, K., E. Chklovskaia, B. Fazekas de St Groth, W. Jessup, and T. Harder. 2005. Condensation of the plasma membrane at the site of T lymphocyte activation. *J. Cell Biol.* 171:121–131.

68. Nishio, M., S. Fukumoto, K. Furukawa, A. Ichimura, H. Miyazaki, S. Kusunoki, T. Urano, and K. Furukawa. 2004. Overexpressed GM1 suppresses nerve growth factor (NGF) signals by modulating the intracellular localization of NGF receptors and membrane fluidity in PC12 cells. *J. Biol. Chem.* 279:33368–33378.